Available online at www.sciencedirect.com
ScienceDirect
Agricultural and Forest Meteorology 140 (2006) 136–151
AGRICULTURAL AND FOREST METEOROLOGY
www.elsevier.com/locate/agrformet

Modelling multi-year coupled carbon and water fluxes in a boreal aspen forest

Weimin Ju [a,*], Jing M. Chen [a], T. Andrew Black [b], Alan G. Barr [c], Jane Liu [d], Baozhang Chen [a]

[a] Department of Geography, University of Toronto, Toronto, Ont. M5S 3G3, Canada
[b] Faculty of Land and Food Systems, University of British Columbia, Vancouver, BC, Canada
[c] Climate Research Branch, Meteorological Service of Canada, Saskatoon, SK, Canada
[d] Department of Physics, University of Toronto, Toronto, Ont., Canada

Received 30 November 2005; accepted 7 April 2006

Abstract

In order to test two hypotheses: (i) that carbon (C) and energy exchanges between terrestrial ecosystems and the atmosphere are closely constrained by soil water availability, and (ii) that vegetation is able to optimize soil water uptake from different soil layers; two model simulations were conducted. The Boreal Ecosystem Productivity Simulator (BEPS) model was run to simulate an aspen forest in Saskatchewan, Canada during the period 1997–2004. In Simulation 1, the effect of soil water availability in different soil layers on stomatal conductance was weighted only by root fraction. In Simulation 2, the influence of soil water availability in different soil layers on stomatal conductance was weighted according to both the root fraction and soil water availability, in order to allow easier access of roots to soil layers containing more water.

Comparison against measured fluxes showed that Simulation 2 was an improvement over Simulation 1 in predicting C, water and energy fluxes at different time scales in dry years. In Simulation 1, the daytime C and water fluxes were underestimated during the transition from adequate to insufficient soil water content in the upper layers. In this run, the model captured 92, 79 and 91% of the daily variances in gross primary productivity (GPP), net ecosystem productivity (NEP), and ecosystem respiration (R_e) during 1997–2004. In Simulation 2, the daily variances of GPP, NEP, and R_e explained by the model increased to 93, 82 and 92%, respectively. In Simulation 1, the annual NEP was considerably underestimated in the dry years and years with dry periods, with a root mean square error (RMSE) of 45 g C m^{-2} $year^{-1}$ ($n = 8$) from 1997 to 2004. In Simulation 2, the RMSE value of simulated annual NEP was reduced to 14 g C m^{-2} $year^{-1}$, a relatively small value compared with the average NEP of 157 g C m^{-2} $year^{-1}$ during 1997–2004. This suggested that the ability of plant roots to extract water from deep soil layers is critical for the forest to maintain growth when surface layers dried out. Our model results showed that NEP was very sensitive to water conditions at this site. In wet years, heterotrophic respiration was enhanced and NEP was reduced.

Keywords: Simulation; Boreal Ecosystem Productivity Simulator; Terrestrial carbon

1. Introduction

Terrestrial carbon (C) and water cycles are interactively linked at various temporal and spatial scales (Ball et al., 1987; Leuning, 1995; Rodriguez-Iturbe, 2000). The response of C sequestration by terrestrial

* Corresponding author.
E-mail address: juw@geog.utoronto.ca (W. Ju).

0168-1923/$ – see front matter © 2006 Elsevier B.V. All rights reserved.
doi:10.1016/j.agrformet.2006.08.008

ecosystems to soil wetness depends on the response of photosynthesis and heterotrophic respiration to soil water availability. Reliable simulations of terrestrial C balance require careful descriptions of at least following effects of soil water on C sequestration: (i) The canopy water status as affected by soil and atmospheric water status, (ii) the impact of canopy water status on CO_2 fixation (Grant et al., in press), (iii) the influence of soil water on soil C decomposition, fine root dynamics, and root respiration, and (iv) the estimation of soil thermal parameters related to soil water conditions.

Soil water content in the root zone regulates photosynthesis and transpiration through its effect on stomatal conductance (Jarvis, 1976; Harris et al., 2004). Photosynthesis peaks when soil water content is near the field capacity and decreases with the decrease of soil water content from the field capacity to a threshold (typically the wilting point) below which C assimilation stops. This process is less sensitive to soil water content when it is in the range from the field capacity to near the total porosity (i.e., saturation).

The effect of soil water on heterotrophic respiration is not straightforward. Microbial activity is reduced with volumetric soil water content departing from the optimum, typically 0.6 of the total of soil porosity (Parton et al., 1993; Friend et al., 1997; Frolking et al., 2001). Low soil water content values constrain microbial activity and heterotrophic respiration. On the other hand, when soil water content approaches saturation, the low availability of oxygen to microbes restricts microbial activity and respiration rates.

The response of net C sequestration by terrestrial ecosystems to soil wetness depends on the balance between the responses of photosynthesis and heterotrophic respiration to soil water availability. Vegetation types, species, and the vertical distribution of soil C are major factors determining the sensitivity of the C flux to drought (Kljun et al., 2004). Multi-year eddy-covariance measurements, at an aspen forest (SOA) site at the Boreal Ecosystem–Atmosphere Study Southern Study Area (BOREAS SSA)/Boreal Ecosystem Research and Monitoring Sites (BERMS) super site near Prince Albert National Park, Saskatchewan, Canada, showed that net C uptake was more sensitive to drought than that of coniferous forests (Kljun et al., 2004). At this moderately well drained site, ecosystem respiration, mainly heterotrophic respiration, significantly decreased in drought years (Barr et al., 2006). However, at the poorly drained old black spruce site of BOREAS Northern Study Area, ecosystem respiration was enhanced in dry conditions. At this northern site, total ecosystem respiration was mainly controlled by temperature and water table with more than half of the daily variance in the C flux due to water table fluctuations. Lower water table depth induced faster heterotrophic respiration. For this forest, the effect of rising temperature was offset by increased precipitation and higher water table, and this forest switched from a source to a sink for C during 1994 and 2004 (Dunn et al., in press).

Biophysical and biogeochemical models often use microscopic and macroscopic approaches to quantify root water uptake for calculating stomatal conductance and photosynthesis (Feddes and Raats, 2006). The microscopic approach simulates the water flow along the soil–root–leaf–atmosphere pathway, considering not only water potential variation but also the dependence of hydraulic conductivity on water potential along the pathway (Feddes and Raats, 2006). This approach uses a set of differential equations, which are often discretized using bulk hydraulic resistances independent of water potential. Some discretized models of this type consider the radial water flow from soil to roots and the axial flow inside roots (Grant et al., in press). These models calculate water uptake based on water potentials and hydraulic resistances along a soil–root–canopy pathway from single (Williams et al., 1996) or multiple (Wang et al., 2001; Grant et al., 2001) soil layers to single (Wang et al., 2001; Grant et al., 2001) or multiple (Williams et al., 1996) canopy layers. A model intercomparison has demonstrated that these models are able to simulate the soil water stress on stomatal conductance and C fixation at different sites well if the detailed data required for model parameterization are available (Grant et al., in press). These models usually require estimation or input data of root density and length.

Models using the macroscopic approach are generally derived based on empirical data without explicit consideration of processes involving individual roots. This approach simulates the bulk water uptake in each layer in the root zone using an empirical function to quantify the water availability to roots. Models of this kind are developed generally for the purpose of large area applications where either the speed of computation or data availability is of concern (Bonan, 1991; Sellers et al., 1986; Arain et al., 2002; Arora, 2003). Some models of this type calculate the potential root water uptake from a normalized soil water content as well as from the fine root mass and hydraulic conductivity, in order to limit canopy transpiration under water stress (Grote et al., 1998). Other models constrain stomatal conductance as a function of soil water potential (Verseghy et al., 1993; Zierl, 2001). In models with

multiple soil layers, different strategies are adopted to quantify the overall effect of soil water availability of different layers on stomatal conductance and photosynthesis, and to partition transpired water among different soil layers. Some models use the average soil water content (Wigmosta et al., 1994), or the minimum value of soil water suction among all soil layers (Verseghy et al., 1993) to constrain the stomatal conductance. Others use the weighted average of soil water potentials (Sellers et al., 1986) or soil water availability in different layers to estimate the canopy water potential (Bonan, 1991) or to evaluate the effect of soil water availability on photosynthesis (Arora, 2003). Each layer is weighted according to the ratio of its thickness to total rooting depth (Sellers et al., 1986) or its relative root fraction (Bonan, 1991; Arora, 2003). Transpired water is usually partitioned among soil layers within the rooting zone according to layer depth, water availability, or relative root fraction (Sellers et al., 1986; Abramopoulos et al., 1988; Verseghy et al., 1993; Chen et al., 2005).

Models, which evaluate the overall effect of water availability on the basis of root distribution, have the potential to overestimate the reductions of stomatal conductance, photosynthesis and transpiration caused by drought during the period of drought onset. These models tend to give too much weight to the upper layers in calculating the soil water availability factor due to their assumption that root fraction exponentially decreases with depth. When the thinner, upper soil layers dry out, stomata shut down, consequently limiting transpiration and photosynthesis (Prihodko et al., 2005). Measurements show that vegetation has the ability to consume soil water in deeper layers when upper layers dry out (Kljun et al., 2004). During a continuous drought from 2001 to 2003, the SOA forest maintained a normal photosynthesis rate in the first drought year 2001 while ecosystem respiration reduced, producing the highest annual net ecosystem productivity (NEP) in recent 9 recorded years (Griffis et al., 2004; Barr et al., 2004). When deeper layers dried out in the following 2 years, both photosynthesis and heterotrophic respiration decreased. Allowing the vegetation a greater access to deep water is necessary for reliable simulations of water, energy, and C fluxes during dry seasons (Prihodko et al., 2005).

The main purpose of this study is to simulate the multi-year coupling between water and C cycles for the SOA forest and to demonstrate the importance of properly parameterizing the effect of soil water on stomatal conductance for simulating energy and C fluxes at different time scales. The tool used for this research is the updated Boreal Ecosystem Productivity Simulator (BEPS) model, which we briefly describe here prior to presenting our results.

2. Model description

The BEPS model was initially developed to calculate the net primary productivity (NPP) for Canada landmass at 1 km resolution and daily time steps, driven by spatial datasets of climate, remotely sensed vegetation parameters (leaf area index, LAI), land cover type, clumping index), and soil water holding capacity (Liu et al., 2002). Daily C fixation is calculated by scaling Farquhar's leaf biochemical model (Farquhar et al., 1980) up to canopy-level implemented with a spatial and temporal scaling scheme (Chen et al., 1999). Daily gross primary productivity (GPP) is calculated separately for sunlit and shaded leaves (Liu et al., 2002, 2003). The soil water balance is calculated using a one-layer bucket model and soil temperature is not simulated. Soil respiration is calculated using one-C pool method.

This model was recently updated to include a module for photosynthesis calculation (Chen et al., 1999), a soil biogeochemical module for soil C, N and heterotrophic respiration simulations following CENTURY (Parton et al., 1993), and a land surface scheme for the computations of energy balance, sensible and latent heat fluxes, soil water and soil temperature status (Chen et al., submitted for publication). The 'Jarvis' model (Jarvis, 1976) previously used for the calculation of stomatal conductance is replaced, in this study, by a modified version of the Ball–Woodrow–Berry model (Ball et al., 1987). The information flows in the model are presented in Fig. 1. In the model framework, the canopy is stratified into overstory and understory layers. For each of them, C, water, and energy fluxes are simulated separately. Under a seasonal snowpack, the soil profile is split into multiple layers (five were used in this study), for each of them temperature and water content are simulated separately. The number of snowpack layers is adjusted according to snow thickness, which is estimated on the basis of snow density and snow water equivalent. The dynamics of soil C and nitrogen is simulated using a modified version of CENTURY (Parton et al., 1993; Ju and Chen, 2005). Heterotrophic respiration is a function of soil C mass, decomposition rate of soil C and respiration efficiency. Further details of the model can be found in the following publications: Chen et al. (1999, 2005), Ju and Chen (2005). Here, we only outline some of the major methodologies and recent modifications directly related to this study.

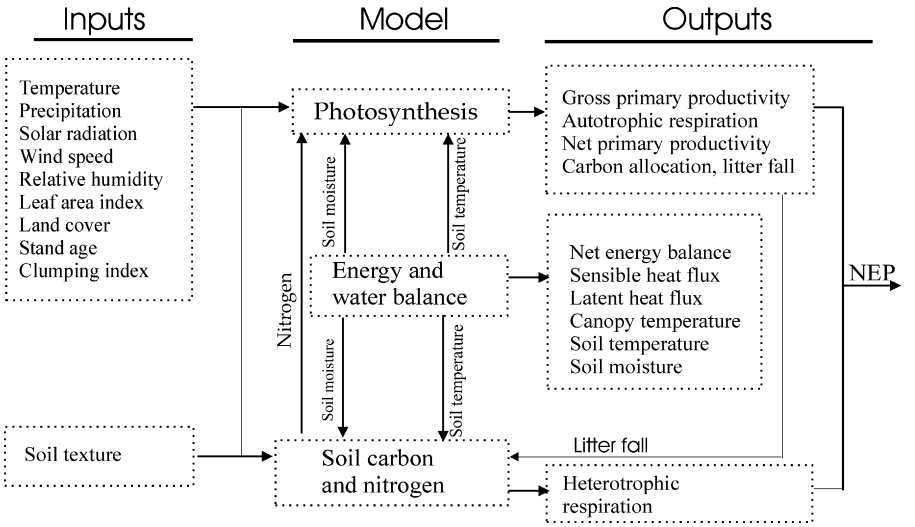

Fig. 1. The major inputs/outputs and information flows in the updated BEPS model.

2.1. Calculation of net ecosystem productivity

NEP is calculated as the difference between photosynthesis and respiration, i.e.

$$\mathrm{NEP} = \mathrm{GPP_o} - R_{\mathrm{ao}} + \mathrm{GPP_u} - R_{\mathrm{au}} - R_{\mathrm{h}} \quad (1)$$

where GPP and R_{a} are the GPP and autotrophic respiration of overstory (o) and understory (u), respectively.

GPP of understory and overstory was calculated using a two-leaf (sunlit and shaded) canopy photosynthesis model (Chen et al., 1999; Liu et al., 2002). The rates of net photosynthesis of sunlit ($i = 1$) and shaded ($i = 2$) leaf fractions are calculated separately as the minimum of:

$$A_{\mathrm{c},i} = V_{\mathrm{m}} \frac{C_{\mathrm{i}} - \Gamma_i^*}{C_{\mathrm{i}} + K_{\mathrm{c}}(1 + \mathrm{O_i}/K_{\mathrm{o}})} \quad (2a)$$

and

$$A_{\mathrm{j},i} = J \frac{C_{\mathrm{i}} - \Gamma_i^*}{4(C_{\mathrm{i}} - 2\Gamma_i^*)} \quad (2b)$$

where $A_{\mathrm{c},i}$ and $A_{\mathrm{j},i}$ are Rubiso-limited and RuBP-limited gross photosynthesis rates ($\mu\mathrm{mol\,m^{-2}\,s^{-1}}$), respectively. V_{m} is the maximum carboxylation rate ($\mu\mathrm{mol\,m^{-2}\,s^{-1}}$); J is the electron transport rate ($\mu\mathrm{mol\,m^{-2}\,s^{-1}}$); C_{i} and O_{i} are the intercellular CO_2 and oxygen concentration ($\mathrm{mol\,mol^{-1}}$), respectively; Γ_i^* is the CO_2 compensation point without dark respiration ($\mathrm{mol\,mol^{-1}}$); K_{c} and K_{o} are Michaelis–Menten constants for CO_2 and O_2 ($\mathrm{mol\,mol^{-1}}$), respectively.

The rates of net photosynthesis rate is calculated as

$$A_{\mathrm{net},i} = \min(A_{\mathrm{c},i}, A_{\mathrm{j},i}) - R_{\mathrm{d}} \quad (3)$$

where R_{d} is the daytime leaf dark respiration and computed as $R_{\mathrm{d}} = 0.015V_{\mathrm{m}}$.

The bulk stomatal conductance of the sunlit and shaded leaves for water vapor ($G_{\mathrm{s},i}$, $\mathrm{mol\,m^{-2}\,s^{-1}}$) is calculated using a modified version of the Ball–Woodrow–Berry (Ball et al., 1987) empirical model following Wang and Leuning (1998):

$$G_{\mathrm{s},i} = G_{\mathrm{o},i} + \frac{a f_{\mathrm{w}} A_{\mathrm{net},i}}{C_{\mathrm{s},i}(1 + D_{\mathrm{s},i}/D_0)} \quad (4)$$

where $G_{\mathrm{o},i}$ is the residual conductance ($\mathrm{mol\,m^{-2}\,s^{-1}}$); $C_{\mathrm{s,i}}$ is the CO_2 concentration at the leaf surface ($\mu\mathrm{mol\,mol^{-1}}$); $D_{\mathrm{s},i}$ is the water vapor saturate deficit at the leaf surface (kPa); D_0 is an empirical parameter determining the sensitivity of stomatal conductance to water vapor saturate deficit (kPa), a is a parameter related to the intercellular CO_2 concentration by $C_{\mathrm{i}}/C_{\mathrm{s,i}} = 1 - 1/a$ at maximal stomatal opening (when both $D_{\mathrm{s},i}$ and $G_{0,i}$ are zero and $f_{\mathrm{w}} = 1$); f_{w} is a parameter describing the sensitivity of $G_{\mathrm{s},i}$ to soil water availability (see Section 2.3).

The diffusion of CO_2 from the atmosphere into the leaf is described by

$$A_{\mathrm{net},i} = 0.64 G_{\mathrm{s},i}(C_{\mathrm{s,i}} - C_{\mathrm{i}}) = C_{\mathrm{c,i}}(C_{\mathrm{a}} - C_{\mathrm{i}}) \quad (5)$$

where the constant 0.64 is the ratio of the molecular diffusivity of CO_2 to that of water; C_{a} is the ambient CO_2 concentration ($\mu\mathrm{mol\,mol^{-1}}$); $C_{\mathrm{c,i}}$ is the total

conductance for CO_2 from the intercellular space of the leaves to the reference height above the canopy (mol m^{-2} s^{-1}).

Above Eqs. (2)–(5) and the leaf energy balance equations are solved iteratively for $A_{net,i}$, $G_{s,i}$, C_i, $C_{s,i}$, $D_{s,i}$ and leaf temperatures. The iteration will stop when difference of temperature values between two successive iteration is <0.01 °C for either sunlit or shaded leaves (Wang and Leuning, 1998).

2.2. Respiration calculation

Autotrophic respiration (R_a) is separated in two growth respiration (R_g) and maintenance respiration (R_h) components. Growth respiration is calculated as 20% of GPP while maintenance respiration is temperature dependent:

$$R_m = \sum_{i=1}^{4} R_{m,i} = \sum_{i=1}^{4} M_i r_{m,i} Q_{10}^{(T-T_b)/10} \quad (6)$$

where i is an index for different plant parts (1 for leaf, 2 for stem, 3 for coarse root, and 4 for fine root); M the biomass (sapwood for stem) (kg m^{-2}); $r_{m,i}$ the respiration rate at the base temperature T_b (°C) and T is temperature.

The sensitivity of maintenance respiration to temperature (Q_{10}) is now a function of temperature following Arora (2003), i.e.

$$Q_{10} = 3.22 - 0.046T \quad (7)$$

In Eq. (1), R_h is the heterotrophic respiration and is computed as the sum of C released to the atmosphere during the decomposition of five litter (surface structural litter, surface metabolic litter, soil structural litter, soil metabolic litter, and coarse woody litter) and four soil C (surface microbe, soil microbe, slow, and passive) pools, i.e.

$$R_h = \sum_{j=1}^{9} \tau_j k_j C_j \quad (8)$$

where τ_j is a respiration efficiency equal to the percentage of decomposed C released from pool j to the atmosphere, k_j the decomposition rate of C pool j and C_j is the size of pool j and is updated at each time step.

The decomposition rate of each C pool is equal to the maximum value regulated by the stress factors of soil water, temperature, lignin content (for litter pools) and soil texture (for the soil microbial pool). The stress factor of soil temperature is calculated using a modified Arrhenius-type equation (Lloyd and Taylor, 1994) and the stress factor of soil water $f(\theta)$ is quantified as (Potter, 1997):

$$f(\theta) = \begin{cases} 5.44\left(\frac{\theta}{P}\right) - 5.03\left(\frac{\theta}{P}\right)^2 \\ \quad - 0.492 \quad \text{coarse texture soils} \\ 5.63\left(\frac{\theta}{P}\right) - 4.64\left(\frac{\theta}{P}\right)^2 \\ \quad - 0.745 \quad \text{medium and fine texture soils} \end{cases} \quad (9)$$

where θ is the volumetric soil water content and P is the soil porosity, which is estimated from soil texture. At very dry or near saturation conditions, $f(\theta)$ takes on a value of 0.2.

It is assumed that the decomposition rates of surface structural, surface metabolic, and surface microbial C pools are controlled by temperature and water conditions in the uppermost soil layer. The decomposition rates of other C pools are determined by the weighted average of stress factors of soil temperature and water in deeper layers (Ju and Chen, 2005). The weight of each layer determining the stress factor decreases with depth from the surface in a similar vertical distribution pattern with soil C content.

2.3. Parameterization of root water extraction: Simulation 1 versus Simulation 2

A macroscopic approach for root water uptake estimation is adopted in BEPS as it was developed for large area applications based on remote sensing. In this approach, the rate of root water uptake is directly proportional to the soil water availability to roots. Soil water availability factor $f_{w,i}$ in each layer is calculated as:

$$f_{w,i} = \frac{1.0}{f_i(\psi_i) f_i(T_{s,i})} \quad (10)$$

where $f_i(\psi_i)$ is a function of water suction ψ_i (m) and computed as (Zierl, 2001):

$$f_i(\psi_i) = \begin{cases} 1.0 + \left[\frac{(\psi_i - 10.0)}{10.0}\right]^{\alpha} & \psi_i > 10 \\ 1.0 & \text{else} \end{cases} \quad (11)$$

where α is an empirical parameter determining the sensitivity of stomatal conductance to soil water availability. This function increases with increasing water suction in the soil, resulting in less soil water availability to roots (decreasing $f_{w,i}$). This simple function is effective in scaling the relative effects of water potential on root water uptake in different soil layers. When

detailed root data are available, the approach of Grant et al. (2001, in press) to estimating root radial and axial hydraulic resistances in each layer could be an improvement. However, these hydraulic resistances should also depend on soil water potential in order to accurately simulate water uptake in different layers.

The effect of soil temperature on soil water uptake is described following Bonan (1991):

$$f_i(T_{s,i}) = \begin{cases} \dfrac{1.0}{[1-\exp(t_1 T_{s,i}^{t_2})]} & T_{s,i} > 0^\circ C \\ \infty & \text{else} \end{cases} \quad (12)$$

where t_1 and t_2 are two parameters determining the sensitivity of water uptake by roots to soil temperature.

In most models, the weighting of each soil layer w_i is determined according to root fractions:

$$w_i = \frac{R_i}{\sum_{i=1}^{n} R_i} \quad (13)$$

where R_i is the root fraction in layer i.

Eq. (13) gives large weights to the upper soil layers since the root fraction decreases exponentially with depth. When these thin layers dry out, stomatal conductance decreases greatly, and photosynthesis and transpiration decrease correspondingly. Observations showed that vegetation used deep soil water to maintain photosynthesis and respiration even when soil water content in upper soil layers became very low (Arya et al., 1975; Nnyamah and Black, 1977; Kljun et al., 2004; Prihodko et al., 2005). Modeling studies suggested that deep soil layers are primarily responsible for the total water uptake within the root zone when the top soil layers approach the wilting point (Lai and Kaul, 2000). In order to remove this weakness of Eq. (13), we used a new method to calculate the weight of each layer:

$$w_i = \frac{R_i f_{w,i}}{\sum_{i=1}^{n} R_i f_{w,i}} \quad (14)$$

The overall soil water availability f_w of the whole soil profile used in Eq. (4) is:

$$f_w = \sum_{i=1}^{n} f_{w,i} w_i \quad (15)$$

The main purpose of Eq. (14) is to allow vegetation to optimize the use of its energy by extracting water preferentially from soil layers that require the lowest levels of energy (Radcliffe et al., 1980). The combination of root distribution and soil water availability in calculating water stress factor is important in simulating the root water uptake, soil water content, and energy and carbon fluxes (Li et al., 2001; Prihodko et al., 2005).

The transpired water will be partitioned among soil layers according to w_i. Our partition method (Eq. (14)) is similar to that of Jassal et al. (2004), but we consider the additional effect of the temperature vertical gradient on water uptake (Eq. (12)). This temperature effect is particularly important at the beginning of the growing season in boreal ecosystems.

For convenience, we will refer to the model run using Eq. (13) as Simulation 1 and the run using Eq. (14) as Simulation 2.

2.4. Improved description of soil hydraulic and thermal properties

At high latitudes, soils undergo freezing and thawing periods, which affect the movement of water and heat. A modelling experiment has shown that an improved representation of soil freezing curve results in a better simulation of the movement of the melting front through the peat and improves the simulation of the above-ground fluxes (Hall et al., 2003). In the current BEPS model, the influences of freezing and thawing in soils on hydrologic and thermal properties are explicitly described. The detailed descriptions about the calculations of soil water and temperature are given in Chen et al. (submitted for publication). Only the recent modifications are given here.

For the ith soil layer of thickness D_i (m) at temperature $T_{s,i}$, the heat balance is given by

$$C_{A,i} D_i (T_{s,i}^{t+1} - T_{s,i}^{t}) = G_{i-1} - G_i - J_i D_i \quad (16)$$

where $C_{A,i}$ is the apparent volumetric heat capacity of layer i (J m^{-3} K^{-1}), D_i the thickness of layer i (m), G is diffusive heat flux (W m^{-2}) and J_i is the net heat flux (W m^{-3}) associated with soil water flux (Hall et al., 2003).

The apparent volumetric heat capacity $C_{A,i}$ is given by:

$$C_A = \rho_s c_{ps} \theta_s + \rho_w c_{pw} \theta_u + \rho_i c_{pi} \theta_i + L_f \frac{\partial \theta_u}{\partial T_s} \quad (17)$$

where ρ is the density (kg m^{-3}), c_p the specific heat capacity (J kg^{-3} K^{-1}), θ the volumetric content (m^3 m^{-3}), and L_f is the latent heat of fusion for ice (J kg^{-1}). Subscripts s, u, i denote solid particles, unfrozen water, and ice, respectively.

The diffusive soil heat flux between the boundary of layers $(i-1)$ and i is determined by:

$$G_i = \frac{(T_{s,i-1} - T_{s,i})}{0.5 D_{i-1}/\lambda_{i-1} + 0.5 D_i/\lambda_i} \quad (18)$$

where λ is the thermal conductivity of the soil (W m^{-1} K^{-1}) and computed as (Cote and Konrad, 2005):

$$\lambda = (\lambda_{sat} - \lambda_{dry}) \frac{\beta S_r}{1 + (\beta - 1) S_r} + \lambda_{dry} \quad (19)$$

where λ_{sat} and λ_{dry} are the thermal conductivity of saturated and dry soils (W m^{-1} K^{-1}), respectively; β is an empirical parameter accounting for the sensitivity of the thermal conductivity to the degree of saturation in the unfrozen and frozen states; and S_r is the degree of saturation.

The thermal conductivity λ_{dry} of a totally dry soil is calculated using the method of Cote and Konrad (2005):

$$\lambda_{dry} = \chi 10^{-\eta P} \quad (20)$$

where χ (W m^{-1} K^{-1}) and η (unitless) are material parameters accounting for the particle shape effects, respectively. They are 0.75 and 1.2 for mineral soils and 0.3 and 0.87 for organic peat soils, respectively.

The thermal conductivity of a saturated soil λ_{sat} is calculated as:

$$\lambda_{sat} = k_s^{1-P} k_i^{P-\theta_u^{max}} k_w^{\theta_u^{max}} \quad (21)$$

where k_s, k_i, and k_w are the thermal conductivities of solid particles, ice, and unfrozen water, respectively; θ_u^{max} is the maximum volumetric fraction of liquid water that can exist in the frozen soil.

The thermal conductivities of solid particles k_s is computed as:

$$k_s = 7.7^{f_{sand}} 2.9^{f_{silter}} 2.9^{f_{clay}} 0.25^{f_{org}} \quad (22)$$

where f_{sand}, f_{silt}, f_{clay}, and f_{org} are volumetric fractions of sand, silt, clay, and organic matter, respectively.

In a frozen soil, the maximum liquid water content is determined by temperature T_s and soil texture (Hall et al., 2003):

$$\theta_u^{max} = P \left[-\alpha \frac{\rho_i L_f (T_s - T_0)}{\rho_w T_0 g \psi_s} \right]^{-1/b}, \quad \text{if} \quad T_s < T_0 \quad (23)$$

where P is porosity (m3 m^{-3}), α the dimensionless constant with a value that depends on soil texture, g (m s^{-2}) the acceleration due to gravity, ψ_s (m of water) the air entry matric potential, and b is an empirical exponent, depending on soil texture; $T_0 = 273.15$ °K.

The actual value of volumetric liquid soil water content (VLSWC) θ_u is limited by the total water content of the soil θ, so that:

$$\theta_u = \min(\theta_u^{max}, \theta) \quad (24)$$

3. Description of site and data

In this study, we ran the model for a 73-year-old, 22-m-tall trembling aspen (*Populus tremuloides* Michx) forest. It is located in the BOREAS SSA/BERMS study area (53.6°N, 106.2°W). The forest canopy has two distinct layers: overstory aspen leaves are confined to the top 5–6 m of the stand and a hazelnut (*Corylus cornuta* Marsh.) understory is about 2 m tall with leaves distributed throughout. The stem density is about 860 ha^{-1}. The LAI values have considerable inter-annual variability, ranging from 1.95 to 2.53 for the overstory and from 1.96 to 2.80 for the understory during 1994–2004 (Barr et al., 2004; Chen et al., 2006). Mean annual air temperature and precipitation at the nearest long-term weather station are 0.5 °C and 406 mm, respectively. In recent years, the climate at this site was on average 1.5 °C warmer and slightly drier than the climate normal (Barr et al., 2004). The soil is an Orthic Gray Luvisol with 8–10 cm deep surface organic layer overlying a loam to sandy loam mineral soil (Table 1). The terrain is generally level.

Half-hourly measurements of climate variables, including air temperature, incoming solar radiation, downward long wave radiation, relative humidity, and wind speed at 37 m were used to continuously drive the model from 1997 to 2004. Measurements of energy and CO_2 fluxes using the eddy covariance method (Griffis et al., 2003), soil temperature, and soil water content were used for model validation and sensitivity analysis. Half-hourly or 6-hourly measurements were summed or averaged to produces daily and annual values for model validation. The CO_2 fluxes had been gap-filled and corrected for the underestimation of respiratory fluxes on calm nights (Barr et al., 2004). These gap-filled data are used for annual statistics but not for validating half-hourly and daily model simulations. For other variables with gaps, daily values were only calculated for days with more than 36 half-hourly measurements. Observed biomass was used to estimate autotrophic respiration.

Measured midsummer maximum LAI values were used to drive the model. The course of LAI was estimated according to air temperature. Leaf emergence was determined according to growing degree days (GDD), which is the difference between daily mean air temperature and a threshold of 5 °C. Leaf emergence occurred when the accumulated GGD reached 75 °C d. After emergence, the increase in LAI was linearly related to the increase in GDD. When the accumulated GDD reached 500 °C d, the development of canopies was completed. LAI was set to the measured value after

Table 1
Soil characteristics[a] and parameters used in the land surface scheme module

Parameter	Layer 1	Layer 2	Layer 3	Layer 4	Layer 5	Reference
Thickness D (m)	0.05	0.1	0.2	0.4	1.5	This study
Bulk density (Mg m^{-3})	0.12	0.19	1.38	1.53	1.67	Grant et al. (in press)
Sand fraction (g kg^{-1})	0	0	590	570	480	Grant et al. (in press)
Silt fraction (g kg^{-1})	0	0	290	230	280	Grant et al. (in press)
Clay fraction (g kg^{-1})	0	0	120	200	240	Grant et al. (in press)
Organic C fraction (g kg^{-1})	430	313	6.2	3.4	3.4	Grant et al. (in press)
Air entry suction ψ_s (m of water)	0.05	0.06	0.16	0.20	0.23	This study
Saturated hydraulic conductivity k_s (10^{-6} m s^{-1})	2	4	6	1.5	1.0	This study
Wilting point (m^3 m^{-3})	0.15	0.15	0.07	0.13	0.13	Grant et al. (in press)
Field capacity (m^3 m^{-3})	0.62	0.62	0.17	0.23	0.21	Grant et al. (in press)
Porosity, P (m^3 m^{-3})	0.89	0.85	0.48	0.50	0.50	This study
Empirical exponent b	3.6	3.6	3.6	4.0	4.0	This study
Parameter for thermal conductivity calculation β (frozen)	0.12	0.80	1.6	1.5	1.5	This study
Parameter for thermal conductivity calculation β (unfrozen)	0.42	2.0	4.0	4.0	4.0	This study
Parameter for maximum liquid water content in frozen soils α	0.06	0.06	0.06	0.01	0.01	This study

[a] Anderson, D. 1998. BOREAS TE-01 Soils Data over the SSA Tower Sites in Raster Format, Available online at [http://www-eosdis.ornl.gov/] from the ORNL Distributed Active Archive Center, Oak Ridge National Laboratory, Oak Ridge, Tennessee, U.S.A.

this day and then stabilized until the senescence initiated. The leaf fall was completed when the accumulated negative GDD below a threshold of 5 °C exceeded −5 °C d. The last day of senescence was restricted in the range of 265–275 days of the year. The senescence starts 2 weeks prior to the last day.

4. Model parameterization, initialization and simulations

4.1. Model parameterization and initialization

The BEPS model was continuously run for years from 1997 to 2004. The values of model parameters for the land surface scheme and the photosynthesis modules are summarized in Table 2 together with their sources. The model was run twice. The first run was for the initialization of the second run. From simulated half-hourly soil temperature and water content, half-hourly stress factors for soil C decomposition were calculated and averaged over the period from 1997 to 2004 to calculate the annual mean of decomposition rates of soil C pools. The sizes of C pools prior to 1997 were initialized using the mean decomposition rates and an incremental stand age (Ju and Chen, 2005). The measured soil C density data was used for calibrating the initialization. Measured biomass data were used for calculating autotrophic respiration. The initial values of snow depth, soil temperature, soil water content, canopy temperature were set to the observed values for 1 January of 1997. In the second run, the size of each soil C pool was updated at each time step.

4.2. Simulations of soil water content and soil temperature

Soil temperature and water affect soil respiration and canopy conductance. Therefore, the accuracy of simulated energy, C and water fluxes depends, to large extent, on how these two variables are reliably simulated. Fig. 2 shows the comparison between simulated daily

Table 2
Values of parameters in stomatal and photosynthesis models

Symbol	Unit	Description	Values	Reference
Ω	–	Clumping index	0.85	This study
V_{max}	(μmol m^{-2} s^{-1})	Maximum carboxylation rate at 25 °C	60	Arain et al. (2002)
$G_{0,i}$	(mol m^{-2} s^{-1})	Residual conductance	0.01	Wang and Leuning (1998)
a	–	Parameter related to intercellular CO_2	8.0	Arain et al. (2002)
D_0	kPa	Parameter for stomatal sensitivity to VPD	1.5	Wang and Leuning (1998)
α	–	Sensitivity of soil water uptake to water potential	0.8	This study
t_1	–	Sensitivity of soil water uptake to temperature	−0.04	Bonan (1991)
t_2	–	Sensitivity of soil water uptake to temperature	2.0	Bonan (1991)

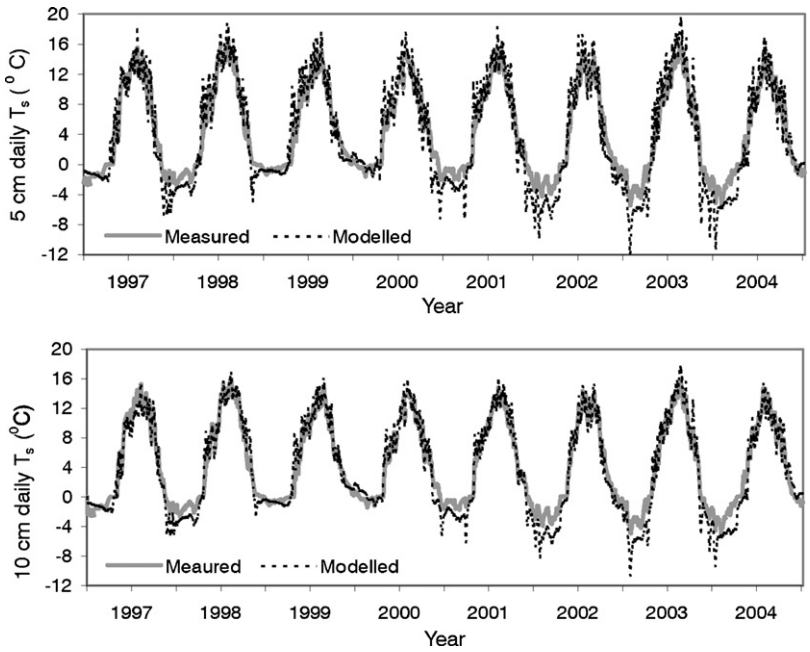

Fig. 2. Daily mean soil temperatures at the 5- and 10-cm depths simulated in Simulation 2 compared with measurements during 1997–2004. Daily values are averaged from half-hourly simulations and observations.

mean soil temperatures from Simulation 2 and observations at the 5- and 10-cm depths. In general, the model was able to capture the seasonal, annual variations of soil temperature. The variance of daily mean soil temperature explained by the model was 0.93 (root mean square error (RMSE) = 2.0 °C, n = 2856) at 5 cm and 0.96 (RMSE = 1.5 °C, n = 2856) at 10 cm from 1997 to 2004. Simulated soil temperatures in the upper layers had larger diurnal

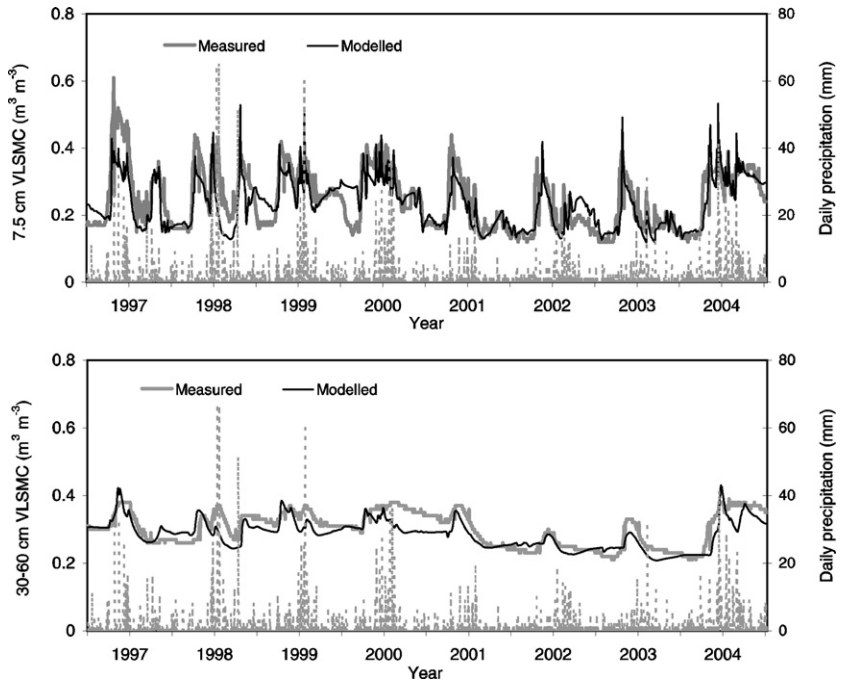

Fig. 3. Comparison between simulated (Simulation 2) and measured daily volumetric liquid soil water contents (VLSWC) at 7.5- and 30–60-cm depths during 1997–2004. The dotted line denotes precipitation.

Table 3
Statistics from the regression ($Y = aX + b$) of simulated (as Y) on observed (as X) half-hourly energy fluxes (W m^{-2}) and net ecosystem CO_2 fluxes (μmol C m^{-2} s^{-1})

Item	Year	Simulation 1				Simulation 2				N
		a	b	R^2	RMSE	a	b	R^2	RMSE	
Latent heat LE	1999	0.90	14.51	0.81	28.63	0.91	14.65	0.81	28.91	16053
	2000	0.79	10.02	0.80	25.91	0.81	10.17	0.80	25.92	14321
	2001	0.81	7.75	0.81	27.66	0.87	8.40	0.83	26.15	14744
	2002	0.74	10.52	0.69	27.73	0.77	10.55	0.70	27.33	14714
	2003	0.79	10.75	0.67	28.21	0.82	10.64	0.68	27.51	13873
	2004	0.89	14.05	0.78	26.70	0.91	14.10	0.78	26.60	15634
Sensible H	1999	0.98	7.18	0.89	35.05	0.98	6.88	0.89	34.81	16101
	2000	1.12	6.45	0.81	54.41	1.11	6.15	0.81	54.27	14489
	2001	1.16	9.79	0.83	54.77	1.13	8.25	0.84	52.16	14486
	2002	1.02	12.37	0.77	62.05	1.01	11.62	0.77	61.46	14814
	2003	1.03	5.67	0.82	55.49	1.02	5.26	0.83	54.96	12954
	2004	0.90	1.777	0.75	53.06	0.89	−2.10	0.74	53.31	15815
Net primary productivity NEP	1997	0.78	−0.07	0.79	3.01	0.82	0.09	0.81	2.85	11832
	1998	0.90	0.09	0.81	2.86	0.90	0.09	0.81	2.86	11057
	1999	0.84	0.17	0.80	2.71	0.84	0.17	0.80	2.72	12744
	2000	0.82	0.10	0.83	2.38	0.83	0.11	0.82	2.41	11062
	2001	0.83	0.01	0.82	2.82	0.86	0.22	0.84	2.69	12029
	2002	0.85	−0.02	0.82	2.22	0.87	0.06	0.82	2.17	12219
	2003	0.84	−0.23	0.79	2.55	0.86	−0.03	0.80	2.45	10619
	2004	0.88	0.05	0.82	2.20	0.89	0.01	0.82	2.23	12361

and day-to-day variability than observations (Fig. 2a). It suggests that the model transfers heat too quickly at the ground surface. This problem exists in other models using one-dimensional differential soil heat flow equation (Arain et al., 2002). If thermal conductivity of the first layer was reduced, the simulated temperature was sometimes too low. In this study, the thermal conductivity was calculated with considerations of soil water content, freezing and thawing processes, as well as soil texture. The upper boundary condition of the heat flux was determined according to the solution of an energy balance equation.

The seasonality of soil temperature was successfully captured. The departure of simulated soil temperature from the observations was smaller at 10 cm depth than at 5 cm depth. The model tended to underestimate soil temperature when air temperature dropped dramatically in winter. For example, in winters of 2001–2003, the simulated daily soil temperature was about 5 °C lower than the observations. Fortunately, this site was usually frozen in winter. The bias in simulated soil temperature had a relatively small influence on simulated annual NEP. This model error for simulating soil temperature in winter was related to estimated thermal properties of

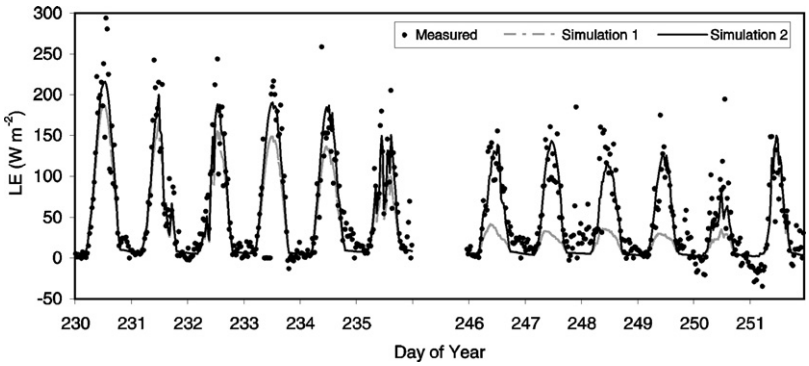

Fig. 4. Comparison of simulated half-hourly latent heat (LE) fluxes from two simulations with measured values during the transition from adequate to deficit soil water content in 2001.

snow. Reducing thermal conductivity by 20% removed this underestimation of soil temperature during these three winters. However, the reduction of snow thermal conductivity caused the overestimation of soil temperature in other winters, suggesting that there is an issue of considering the temporal variability of the thermal conductivity of snow. This model calculates snow thermal conductivity according to its density, which is assumed to increase exponentially with time from accumulation (Verseghy, 1991). The effects of wind speed and temperature on snow compacting have not been included yet. More detailed simulation of snow dynamics may improve the reliability of temperature simulation.

The simulated seasonality of soil temperature was sensitive to the α value of the soil freezing curve (see Eq. (23)), which determines the maximum liquid water content $\theta_u^{\max}$ and the apparent heat capacity C_A at a given temperature in frozen soils. The position of the ice/no ice interface was determined by Eq. (23), which relates actual temperature to unfrozen fraction of soil water. In this formula, most parameters can be determined according soil properties. The only exception to this was the parameter α. A large value of α gave rise to a deep ice/no ice interface and slow melting in spring. Derived by least squares fitting to the observational data, the value of this parameter was found to be 0.06 for organic layers and 0.01 for mineral layers, much larger than the suggested value of 0.005 based on model simulations by Hall et al. (2003) for a peatland in northern Finland. Unfortunately, there is still no physically based method to predict this parameter, and therefore we derived it through model calibration using measured soil temperature data.

At this site, the surface VLSWC exhibited notable seasonal and interannual variability. VLSWC usually increased after snowmelt and then decreased due to transpired and evaporated water exceeding rainfall infiltration. The years 2000 and 2004 were exceptions, when VLSWC was relatively constant during the whole growing seasons. In these two summers, temperature was low and rainfall was abundant. Measured VLSWC was normally low and had small interannual variability between winters. During the continuous drought from 2001 to 2003, VLSWC was lower than the normal, and even deep VLSWC also gradually decreased (Fig. 3).

Fair agreement was found between the observed and simulated VLSWC values from Simulation 2. The model captured 64% of daily variance of VLSWC at 7.5 cm and 72% of daily variance of VLSWC at 30–60 cm, respectively. The model successfully simulated interannual variances of VLSWC in upper and deep soil layers (Fig. 3). The simulated VLSWC at 7.5 cm fluctuated following the infiltration from snowmelt and rainfall while the observed fluctuations of VLSWC were quite small. The quick rise of VLSWC in spring and the decrease of VLSWC in summer at 7.5 cm were well simulated. This indicates that processes of snow melting, soil thaw, and infiltarton were reasonably described. In winter, the model sometimes overestimated VLSWC due to the error in simulating soil temperature. When soil was frozen, VLSWC was estimated as the minimum of the value calculated from (Eq. (23)) and the total volumetric

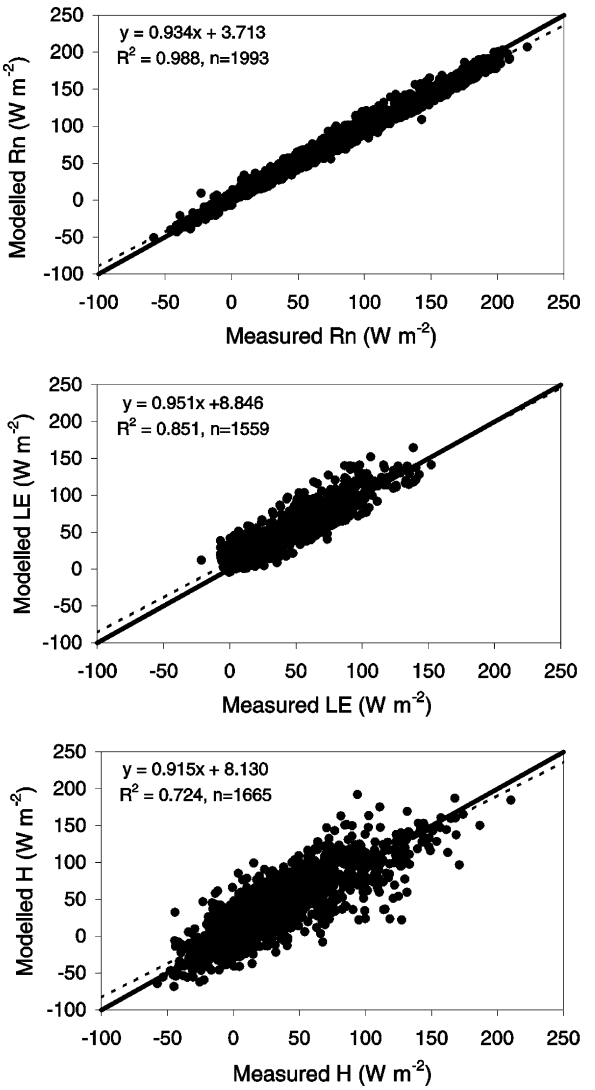

Fig. 5. Regressions between modeled and measured daily mean net radiation above the canopy (R_n), latent heat (LE) and sensible heat (H) fluxes from 1997 to 2004. In this simulation, the effect of soil water content and temperature on stomatal conductance is parameterized using a new algorithm (Simulation 2). The solid line is the 1:1 line and dashed one is the regression line.

soil water content. A small error in simulated soil temperature caused a considerable bias in the simulated VLSWC.

4.3. Comparison of simulated energy fluxes

Simulated energy fluxes during 1999–2004 were compared with measurements at half-hourly and daily time steps. The regression statistics for each study year are summarized in Table 3. In Simulations 1 and 2, the RMSE of simulated latent heat (LE), and sensible heat (H) were in the ranges from 26.2 to 28.91 W m^{-2} and from 34.81 to 62.05 W m^{-2}, respectively. The RMSE and R^2 values indicated that the model performance for half-hourly simulated was better for LE than for H. The R^2 values indicate that the improvement of Simulation 2 for energy fluxes over Simulation 1 was mainly in dry years such as 1997, 2001–2003. In 2001, Simulation 2 explained 83% variance of half-hourly LE, 2% higher than Simulation 1. The slope and interception values in Table 3 showed that the model generally underestimated large LE values. The underestimation of LE during midday may be due to the underestimation of stomatal conductance, which is estimated using the Ball–Woodrow–Berry model (Eq. (4)). Errors in determining parameter a, water stress factor f_w and water vapor pressure deficit on the leaf surface can affect the accuracy of calculated stomatal conductance and latent heat flux. This underestimation was more obvious in Simulation 1 than in Simulation 2. When soil water content is sufficient, these two simulations produced similar results.

During the transition from adequate to deficit soil water content, the underestimation of LE was significant in Simulation 1. For example, after DOY 225 in 2001, upper soil layers became very dry while deeper layers were still wet. Measured VLSWC at 7.5 cm depth was below the wilting point from DOY 225 to DOY 245 and then increased marginally above the wilting point after DOY 245. VLSWC at the 15–30 cm depth decreased continuously to below the field capacity. At the same time, VLSWC at 30–60 cm was still above the field capacity. LE was slightly underestimated in Simulation 1 after DOY 230 (Fig. 4). The underestimation was obvious from DOY 245 to DOY 250 when VLSWC at 15–30 cm was below the field capacity. Simulation 2 produced LE estimates that were very close to measurements due to the allowed ability of vegetation to use water in deeper layers. A rainfall on DOY 251 caused a notable increase of VLSWC at 7.5 cm depth, and both Simlautions 1 and 2 captured measured LE well. At the onsets of droughts in 2002 and 2003, Simulation 2 was also better than Simulation 1. However, the difference between these two simulations was smaller in 2002 and 2003 than in 2001. In 2002 and 2003, soil water availability in deeper layers was also low (VLSWC below the field capacity). Under this situation, the improvement of Simulation 2 over Simulation 1 in soil water uptake estimation was reduced.

Fig. 5 shows the comparisons between modeled and observed daily mean net radiation R_n, LE, and H fluxes for Simulation 2. The model explained 99% (RMSE = 7.8 W m^{-2}), 85% (RMSE = 13.1 W m^{-2}), and 72% (RMSE = 23.0 W m^{-2}) of daily variances of R_n, LE and H, respectively. However, it tended to overestimate the small energy fluxes and underestimate the large ones. The errors in the simulations of energy fluxes occurred mainly in rainy days. The model was unable to simulate evaporation of intercepted water with reliable precision. In most cases, simulated LE was too high and simulated H was too low on these days. Mostly, this model underestimated the negative values of LE due to condensation.

The method of weighting the effects of soil water and temperature in different soil layers on stomatal conductance affected the accuracy of simulated LE

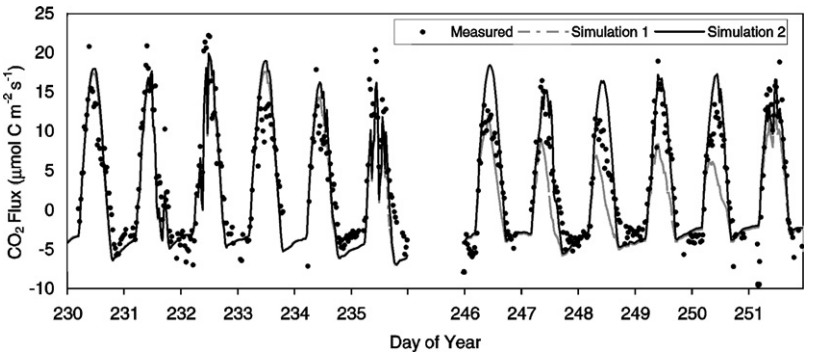

Fig. 6. Comparison of simulated half-hourly CO_2 fluxes from two simulations with measured values during the transition from adequate to deficit soil water content in 2001.

and H. In Simulation 1, the effects of soil water and temperature of different layers were weighted only according to their root fractions (Eq. (13)), and the model-explained variances of daily LE and H were 82% (RMSE = 13.4 W m^{-2}) and 71% (RMSE = 23.7 W m^{-2}), respectively. For example, during the period from DOY 91 to DOY 280 in 2001, the model explained 91% (RMSE = 11.2 W m^{-2}) of the variance of daily LE in Simulation 2, but only 87% of the variance was explained in Simulation 1 (RMSE = 13.5 W m^{-2}). After DOY 231, upper soil layers dried out and measured VLSWC was below the wilting point at 7.5 cm. However, the deep soil layers were still wet and VLSWC was above the field capacity (Fig. 3). The effects of drought were not felt in measured energy fluxes. LE was significantly underestimated in Simulation 1 (Fig. 4), while the new parameterization in Simulation 2 largely remedied this problem.

4.4. Comparison of simulated CO_2 fluxes

In Simulation 1, the model was able to explain 79–83% of the variance of year-round half-hourly NEP during 1997–2004. The RMSE value ranged from 2.20 to 3.01 μmol m^{-2} s^{-1}. In Simulation 2, 80–84% of this variance was captured, and the RMSE value ranged from 2.17 to 2.86 μmol m^{-2} s^{-1}. In 2001, Simulation 2 explained 84% of measured half-hourly variance in NEP, about 2% higher than Simulation 1. In the transition from wet to dry period, the model performed better in Simulation 2 than in Simulation1. Fig. 6 shows a comparison of modelled half-hourly C fluxes from these two simulations with the measured values during the period after the drought onset in 2001. The performance of Simulation 2 also exceeded that of Simulation 1. The difference in NEP simulation is smaller than that in LE simulation since the reduction of photosynthesis caused by water stress was partially offset by the decrease in soil respiration. NEP is less sensitive to soil water availability than LE.

Simulated CO_2 fluxes were also compared with measurements at daily and annually time steps. In Simulation 2, the model was able to simulate GPP, ecosystem respiration (R_e) and NEP under different climate and soil water conditions with reasonable accuracy (Fig. 7). The model explained 93, 82 and 92% of the daily variances in GEP, NEP, and R_e during 1997–2004, respectively. The RMSE values for these three C fluxes were 0.9, 0.9, and 0.7 g C m^{-2} d^{-1}, respectively. Compared with tower data, the model tended to overestimate small GPP values and to underestimate large values of GPP and NEP. The method to evaluate the effect of soil water and temperature on stomatal conductance also affected the accuracy of simulated daily C fluxes. In Simulation 1, the model explained 92, 79, 91% of the daily variances of GPP, NEP, R_e,

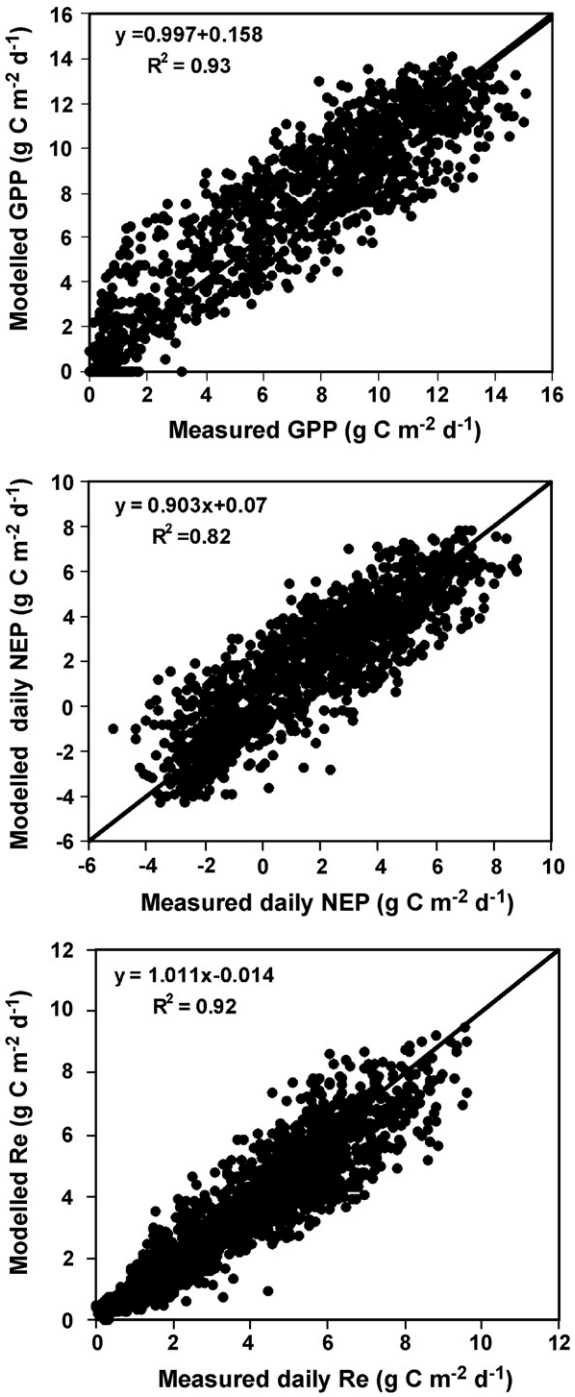

Fig. 7. Comparisons between simulated (Simulation 2) and measured daily GPP, NEP, and ecosystem respiration (R_e) during 1997–2004. The solid line is the 1:1 line.

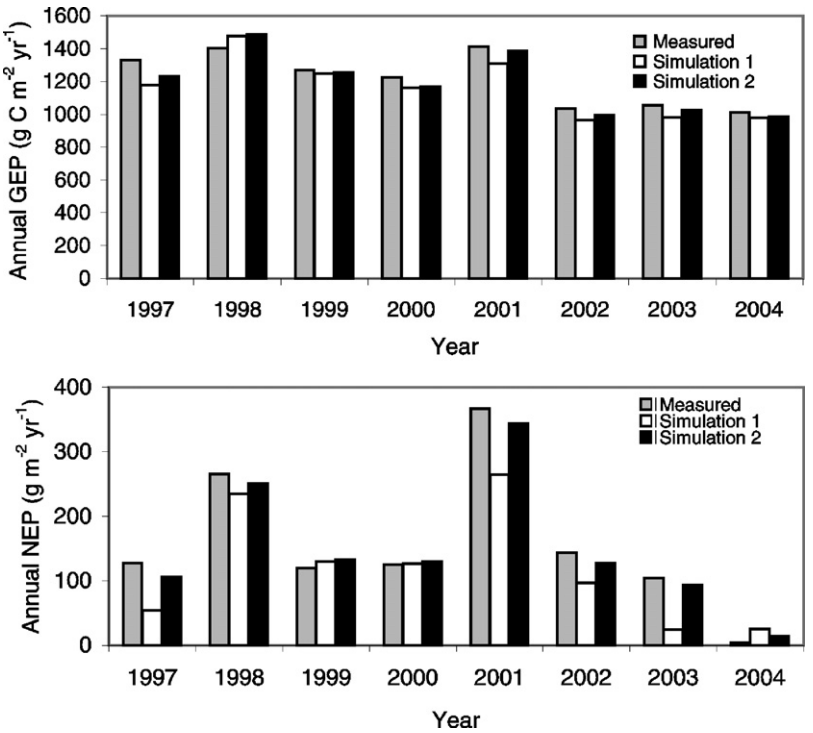

Fig. 8. Comparisons between measured and modelled annual GPP (upper panel) and NEP (low panel) from 1997 to 2004. The model was run twice, using a new method (Simulation 2) and an old method (Simulation 1) to weight the effects of soil water content and temperature of various soil layers on stomatal conductance.

respectively. Simulation 2 was better than Simulation 1 for GPP and NEP simulations due to its better stomatal parameterization against soil water/temperature and roots. The accuracy of simulated R_e was marginally higher in Simulation 2 than in Simulation 1 as it is not directly affected by the stomatal conductance.

The parameterization of the effect of root water uptake on stomatal conductance exerted strong influences on the accuracy of the simulated annual NEP (Fig. 8). In wet years, such as 1999, 2000, and 2004, both Simulations 1 and 2 produced annual values of GEP and NEP close to the measurements. However, in drought years or years with lasting dry periods, Simulation 1 caused considerable underestimation of GPP, and NEP. For example, Simulation 1 gave a value of 264 g C m^{-2} $year^{-1}$ in 2001, considerably lower than the measurement of 365 g C m^{-2} $year^{-1}$. Simulation 2 gave an NEP value of 344 g C m^{-2} $year^{-1}$ in 2001. In 1997 and 1998, the annual precipitation was above normal. However, there were drought conditions in late summer. Upper layers became dry, while soil water was still abundant in deep layers. Under such conditions, Simulation 1 also significantly underestimated annual C sequestration. This confirms the importance of optimizing soil water extraction by vegetation from deep soil layers.

Simulations also showed that heterotrophic respiration at this site had a considerable interannual variability and was more sensitive to precipitation than to temperature. Using a linear regression model, annual precipitation alone explained 67% of the interannual variability of annual heterotrophic respiration (R_h). With temperature added to the regression model, the value only increased to 68%. In wet years, R_h was significantly enhanced. At this site, most new litter and organic C with high decomposition rates concentrate in the top 10 cm of soil (Table 1). At most times, soil water content was lower than the optimum for C decomposition. An increase in soil wetness accelerated the release of soil C to the atmosphere.

5. Summary and conclusions

After introducing a suitable scheme for accessing soil water at various depths by vegetation as well as improving methods of simulating soil temperature and water content, the BEPS model was able to simulate energy and C fluxes at various time scales with reasonable accuracy. From this study, the following conclusions are drawn:

(1) Annual net C sequestration at this forest site was very sensitive to soil water content. The method of calculating the effect of soil water content and temperature on stomatal conductance was found to be very important for the successful simulations of energy and C fluxes at various time scales. The optimization scheme (Simulation 2) considered not only the root fraction but also soil water content and temperature to weight the dependence of stomatal conductance on soil water content and temperature of different soil layers. This markedly improved simulations of C fluxes for a 3-year drought during 2001–2003.
(2) Soil temperature and water both have considerable influences on soil respiration and stomatal conductance. The reliability of calculated soil thermal conductivity is one of the major factors affecting the accuracy of simulated soil temperature. The introduction of a generalized formula for simulating the thermal conductivity based on the degree of saturation, and soil texture and frozen conditions improved the simulation of soil temperature.
(3) At high latitudes, snow cover influences soil temperature, and consequently VLSWC which affects soil C decomposition in winter. A detailed snow model, which tracks the dynamics of snow thermal conductivity, is urgently required for improving simulations of the annual C balance of ecosystems in these regions.
(4) Inclusion of a freezing-curve in a soil temperature module enabled BEPS to accurately simulate the freezing and thawing processes. However, a physically based method has to be developed for determining the α parameter for quantifying the liquid water content at a given soil temperature. Fixed α values were derived through fitting the model to measured temperatures at various depths. These values would be useful for future research on this topic.

Acknowledgement

This research is part of the Fluxnet-Canada Research Network (FCRN) sponsored by the Canadian Foundation for Climate and Atmospheric Sciences, Natural Science and Engineering Council of Canada, and BIOCAP Canada. We gratefully thank Dr. Robert Grant for the provision of soil property data. We acknowledge the work of Zoran Nesic, Andrew Sauter, Rick Ketler, and Shawn O'Neill, who provided laboratory, field and data management support for the flux measurements; Natascha Kljun, Kai Morgenstern and Praveena Krishnan, who assured the quality of the EC data; and Joe Eley, Charmaine Hrynkiw, Dell Bayne, Natasha Neumann, Erin Thompson and Steve Enns, who oversaw the meteorological measurements and data management. We also gratefully acknowledged constructive suggestions by two anonymous reviewers and the editor, which helped improve the quality of manuscript greatly.

References

Abramopoulos, F., Rouseneweig, C., Choudhury, B., 1988. Improved ground hydrology calculation for global climate models (GCMs): soil water movement and evapotranspiration. J. Climate 1, 921–941.

Arain, M.A., Black, T.A., Barr, A.G., Jarvis, P.G., Massheder, J.M., Verseghy, D.L., Nesic, Z., 2002. Effects of seasonal and interannual climate variability on net ecosystem productivity of boreal deciduous and conifer forests. Can. J. Forest Res. 32, 878–891.

Arora, V.K., 2003. Simulating energy and carbon fluxes over winter wheat using coupled land surface and terrestrial ecosystem models. Agric. Forest Meteorol. 118, 21–47.

Arya, L.M., Blake, G.R., Farrell, D.A., 1975. A field study of soil water depletion patterns in presences of growing soybean roots. III. Rooting characteristics and root extraction of soil water. Soil Sci. Soc. Am. Proc. 39, 437–444.

Ball, J.T., Woodrow, I.E., Berry, J.A., 1987. A model predicting stomatal conductance and its contribution to the control of photosynthesis under different environmental conditions. In: Biggins, J. (Ed.), Progress in Photosynthesis Research. Martinus Nijhoff Publishers, Dordrecht, pp. 221–224.

Barr, A.G., Black, T.A., Hogg, E.H., Kljun, N., Morgenstern, K., Nesic, Z., 2004. Inter-annual variability in the leaf area index of a boreal aspen-hazelnut forest in relation to net ecosystem production. Agric. Forest Meteorol. 126, 237–255.

Barr, A.G., Black, T.A., Hogg, E.H., Griffis, T., Morgenstern, K., Kljun, N., Theede, A., Nesic, Z., 2006. Climatic controls on the carbon and water budgets of a boreal aspen forest, 1994–2003. Global Change Biol. 12, 10–16.

Bonan, G.B., 1991. A biophysical surface-energy budget analysis of soil-temperature in the boreal forests of Interior Alaska. Water Resour. Res. 27, 767–781.

Chen, J.M., Liu, J., Cihlar, J., Goulden, M.L., 1999. Daily canopy photosynthesis model through temporal and spatial scaling for remote sensing applications. Ecol. Modell. 124, 99–119.

Chen, J.M., Chen, X.Y., Ju, W.M., Geng, X.Y., 2005. Distributed hydrological model for mapping evapotranspiration using remote sensing inputs. J. Hydrol. 305, 15–39.

Chen, B.Z., Chen, J.M., Ju, W.M. Remote sensing based ecosystem-atmosphere simulation scheme (EASS) Model formulation and test with multiple-year data. Ecol. Modell., submitted for publication.

Chen, J.M., Govind, A., Sonnentag, O., Zhang, Y., Barr, A.G., Amiro, B., 2006. Leaf area index measurements at fluxnet Canada forest sites. Agric. Forest Meteorol. 140, 257–268.

Cote, J., Konrad, J.M., 2005. A generalized thermal conductivity model for soils and construction materials. Can. Geotech. J. 42, 443–458.

Dunn, A.L., Barford, C.C., Wofsy, S.C., Golden, M.L., Daube, B.C. A long-term record of carbon exchange in a boreal black spruce forest: means, response to interannual variability, and long-term trends. Global Change Biol., in press.

Farquhar, G.D., Caemmerer, S.V., Berry, J.A., 1980. A biochemical-model of photosynthetic CO_2 assimilation in leaves of C-3 Species. Planta 149, 78–90.

Feddes, R.A., Raats, P.A.C., 2006. Parameterizing the soil–water–plant root system. In: Fedds, R.A., van Dam, J.C., de'Rooij, G.H. (Eds.), Unsaturated-Zone Modeling: Progress, Challenges and Applications. Kluwer Academic Publisher, pp. 95–141.

Friend, A.D., Stevens, A.K., Knox, R.G., Cannell, M.G.R., 1997. A process-based, terrestrial biosphere model of ecosystem dynamics (Hybrid V3.0). Ecol. Modell. 95, 249–287.

Frolking, S., Roulet, N.T., Moore, T.R., Richard, P.J.H., Lavoie, M., Muller, S.D., 2001. Modeling northern peatland decomposition and peat accumulation. Ecosystems 4, 479–498.

Grant, R.F., Juma, N.G., Robertson, J.A., Izaurralde, R.C., Mcgill, W.B., 2001. Long-term changes in soil carbon under different fertilizer, manure, and rotation: testing the mathematical Model ecosys with data from the breton plots. Soil Sci. Soc. Am. J. 65, 205–214.

Grant, R.F., Zhang, Y., Yuan, F., Wang, S., Gaumont-Guay, D., Hanson, P.J., Chen, J.M., Black, T.A., Barr, A.G., Baldocchi, D.D., Arain, A. Modelling water stress effects on CO_2 and energy exchange in temperate and boreal deciduous forests. Global Biogeochem. Cycles, in press.

Griffis, T.J., Black, T.A., Morgenstern, K., Barr, A.G., Nesic, Z., Drewitt, G.B., Gaumont-Guay, D., McCaughey, J.H., 2003. Ecophysiological controls on the carbon balances of three southern boreal forests. Agric. Forest Meteorol. 117, 53–71.

Griffis, T.J., Black, T.A., Gaumont-Guay, D., Drewitt, G.B., Nesic, Z., Barr, A.G., Morgenstern, K., Kljun, N., 2004. Seasonal variation and partitioning of ecosystem respiration in a southern boreal aspen forest. Agric. Forest Meteorol. 125, 207–223.

Grote, R., Suckow, F., Bellman, K., 1998. Modelling of carbon-, nitrogen- and water-balances in scots pine stands. In: Hüttl, R.F., Bellman, K. (Eds.), Changes of Atmospheric Chemistry and Effect on Forest Ecosystems. Kluwer Academic Publishers, Dordrecht, Netherlands, pp. 251–281.

Hall, R.L., Huntingford, C., Harding, R.J., Lloyd, C.R., Cox, P.M., 2003. An improved description of soil hydraulic and thermal properties of arctic peatland for use in a GCM. Hydrol. Process. 17, 2611–2628.

Harris, P.P., Huntingford, C., Cox, P.M., Gash, J.H.C., Malhi, Y., 2004. Effect of soil moisture on canopy conductance of Amazonian rainforest. Agric. Forest Meteorol. 122, 215–227.

Jassal, R.S., Black, T.A., Drewitt, G.B., Novak, M.D., Gaumont-Guay, D., Nesic, Z., 2004. A model of the production and the transport of CO_2 in soil: predicting soil CO_2 concentration and CO_2 efflux from a forest floor. Agric. Forest Meteorol. 124, 219–236.

Jarvis, P.G., 1976. Interpretation of variations in leaf water potential and stomatal conductance found in canopies in field. Philos. Trans. R. Soc. Lond. Ser. B 273, 593–610.

Ju, W.M., Chen, J.M., 2005. Distribution of soil carbon stocks in Canada's forests and wetlands simulated based on drainage class, topography and remotely sensed vegetation parameters. Hydrol. Process. 19, 77–94.

Kljun, N., Black, T.A., Griffis, T.J., Barr, A.G., Gaumont-Guay, D., Morgenstern, K., McCaughey, J.H., Nesic, Z., 2004. Net carbon exchange of three boreal forests during a drought. In: Proceedings of the 26th Conference on Agricultural and Forest Meteorology, Vancouver, BC, Canada, 12.5, August 23–27.

Lai, C.-T., Kaul, G., 2000. The dynamic role of root-water uptake in coupling potential to actual transpiration. Adv. Water Resour. 23, 427–439.

Leuning, R., 1995. A Critical-appraisal of a combined stomatal-photosynthesis model for C_3 plants. Plant Cell Environ. 18, 339–355.

Li, K.Y., De Jong, R., Boisvert, J.B., 2001. An exponential root-water-uptake model with water stress compensation. J. Hydrol. 252, 189–204.

Liu, J., Chen, J.M., Cihlar, J., 2003. Mapping evapotranspiration based on remote sensing: an application to Canada's landmass. Water Resour. Res. 39, 1189, doi:10.1029/2002WR001680.

Liu, J., Chen, J.M., Cihlar, J., Chen, W., 2002. Net primary productivity mapped for Canada at 1-km resolution. Global Ecol. Biogeogr. 11, 115–129.

Lloyd, J., Taylor, J.A., 1994. On the temperature-dependence of soil respiration. Funct. Ecol. 8, 315–323.

Nnyamah, J.U., Black, T.A., 1977. Rates and patterns of water uptake in a Douglas-fir forest. Soil Sci. Soc. Am. Proc. 41, 972–979.

Parton, W.J., Scurlock, J.M.O., Ojima, D.S., Gilmanov, T.G., Scholes, R.J., Schimel, D.S., Kirchner, T., Menaut, J.C., Seastedt, T., Moya, E.G., Kamnalrut, A., Kinyamario, J.I., 1993. Observations and modeling of biomass and soil organic-matter dynamics for the grassland biome worldwide. Global Biogeochem. Cycles 7, 785–809.

Potter, C.S., 1997. An ecosystem simulation model for methane production and emission from wetlands. Global Biogeochem. Cycles 11, 495–506.

Prihodko, L., Denning, A.S., Baker, I., 2005. Modelling drought tolerance in Amazonia with SiB3. In: Proceedings of the Seventh International Carbon Dioxide Conference, Boulder, Colorado, September 25–30, pp. 683–684.

Radcliffe, D., Hayden, T., Watson, K., Crowley, P., Phillips, R.E., 1980. Simulation of soil-water within the root zone of a corn crop. Agron. J. 72, 19–24.

Rodriguez-Iturbe, I., 2000. Ecohydrology: a hydrologic perspective of climate–soil–vegetation dynamics. Water Resour. Res. 36, 3–9.

Sellers, P.J., Mintz, Y., Sud, Y.C., Dalcher, A., 1986. A simple biosphere Model (SiB) for use within general-circulation models. J. Atm. Sci. 43, 505–531.

Verseghy, D.L., 1991. CLASS-a Canadian land surface scheme for GCMs. I. Soil model. Int. J. Climatol. 11, 111–133.

Verseghy, D.L., Mcfarlane, N.A., Lazare, M., 1993. CLASS-a Canadian land-surface scheme for GCMs. II. Vegetation model and coupled runs. Int. J. Climatol. 13, 347–370.

Wang, S., Grant, R.F., Verseghy, D.L., Black, T.A., 2001. Modelling plant carbon and nitrogen dynamics of a boreal aspen forest in CLASS—the Canadian Land Surface Scheme. Ecol. Modell. 142, 135–154.

Wang, Y.P., Leuning, R., 1998. A two-leaf model for canopy conductance, photosynthesis and partitioning of available energy I: Model description and comparison with a multi-layered model. Agric. Forest Meteorol. 91, 89–111.

Williams, M., Rastetter, E.B., Fernandes, D.N., Goulden, M.L., Wofsy, S.C., Shaver, G.R., Melillo, J.M., Munger, J.W., Fan, S.M., Nadelhoffer, K.J., 1996. Modelling the soil-plant-atmosphere continuum in a Quercus-Acer stand at Harvard forest: the regulation of stomatal conductance by light, nitrogen and soil/plant hydraulic properties. Plant Cell Environ. 19, 911–927.

Wigmosta, M.S., Vail, L.W., Lettenmaier, D.P., 1994. A distributed hydrology-vegetation model for complex terrain. Water Resour. Res. 30, 1665–1679.

Zierl, B., 2001. A water balance model to simulate drought in forested ecosystems and its application to the entire forested area in Switzerland. J. Hydrol. 242, 115–136.